

Density dependence of symmetry energy and neutron skin thickness revisited using relativistic mean field models with nonlinear couplings

C. Mondal^{1,*}

¹*Laboratoire de Physique Corpusculaire, CNRS, ENSICAEN, UMR6534,
Université de Caen Normandie, F-14000, Caen Cedex, France*

The correlation between neutron skin-thickness of a nucleus with neutron excess and density slope parameter of symmetry energy is assessed as a function of density using relativistic mean field models containing non-linear couplings among different mesons. Models with larger skin were found to probe the density slope parameter even at suprasaturation densities, whereas models with smaller skin were observed to be sensitive only at specific subsaturation density, connected to the average density of nuclei. Possible reasons behind this density dependence are explored systematically. These results might be model specific, which need to be reassessed in other type of interactions existing in the literature. Nevertheless, extrapolating the predictions at high densities from models, which are optimized by data at saturation or subsaturation densities, needs to be handled with care.

I. INTRODUCTION

Isovector part of the nuclear interaction poses some unique challenges in the understanding of the nucleonic systems. For example, behaviors of neutron rich nuclei near the drip-line change heavily from the stable nuclei; accurate knowledge about them might facilitate a better understanding of the nucleosynthesis of heavy nuclei [1]. The origin of neutron skins in nuclei with large neutron excess is also attributed to the isospin sensitivity of the nuclear interaction [1–5]. Static properties of neutron stars (NS) *e.g.* mass or radius, as well as the evolution of core collapse supernovae are very sensitive to the neutron-proton asymmetry in the system [6–9]. During the inspiral of a NS-NS merger, the gravitational field of one companion induces a tidal field on the other inducing a tidal deformation. This might be influenced by the neutron-proton content of the system [10]. The knowledge on the possibilities of direct Urca cooling processes [7, 11, 12] hinges on the accurate determination of the proton fraction inside the core of a neutron star; this is clearly influenced by the isovector nature of the nuclear interaction. On these key questions, symmetry energy and its density derivatives can shed some light; finding precise constraints on them is thus imperative to have a better understanding of the isovector part of the nuclear force.

The density dependence of symmetry energy is mostly governed by the density slope parameter L , which is connected to the density (ρ) derivative of the symmetry energy $C_{sym}(\rho)$ as,

$$L = 3\rho \left(\frac{\partial C_{sym}(\rho)}{\partial \rho} \right). \quad (1)$$

Enormous efforts have been made in recent times to constrain the density slope parameter at saturation L_0 ($= L(\rho_0)$, where saturation density $\rho_0 \sim 0.16 \text{ fm}^{-3}$)

and subsaturation ($0.7\rho_0$) densities [3–6, 13–20] from a plethora of different types of experimental quantities. Concerns have been raised recently on constraining further the second order density dependence of symmetry energy, $K_{sym} \left(\sim 9\rho^2 \frac{\partial^2 C_{sym}(\rho)}{\partial \rho^2} \right)$ [21–24], which might play some important roles at the core of a neutron star. The importance of the high density behavior of the symmetry energy in several astrophysical aspects is pointed out in different contemporary calculations [25–31]. However, the density slope parameter is yet to be pinned down decisively. At present, the accepted values of L at saturation lie in between 20 - 100 MeV. This spread is rather large [32]. Most studies on the finite nuclear properties as well as the astrophysical observations including the tidal deformability from GW170817 NS-NS merger event prefer smaller values of L_0 (~ 20 - 60 MeV) [17, 33–36]. A larger value of neutron skin thickness ($\Delta r_{np} = \langle r_n^2 \rangle^{1/2} - \langle r_p^2 \rangle^{1/2}$, with $\langle r_n \rangle^{1/2}$ and $\langle r_p \rangle^{1/2}$ being the root mean square (rms) radii for the neutron and proton distributions, respectively) in ^{208}Pb extracted by Lead (Pb) radius experiment (PREX-I) [37], reinforced recently by PREX-II, however, prefers larger values of $L_0 \sim 80$ - 110 MeV [38]. Further refined results from PREX or upcoming Calcium radius experiment (CREX) [39] will shed more light in this regard. It is worthwhile to mention that extraction of Δr_{np} in ^{208}Pb from different hadronic probes has been made [40–43], although there might be some degree of model dependence involved due to the uncertain regime of quantum chromodynamics.

The extraction of L_0 from neutron-skin thickness of a heavy nucleus was suggested in the early years of the present century [11, 44–49]. An analytic relation was shown by Centelles *et. al.* [4] starting from Droplet model, where various symmetry energy parameters are connected to Δr_{np} of a heavy nucleus. This has been reinforced through a wide variety of mean field models [32], albeit, with a mild presence of model dependence [18]. It has been pointed out in theoretical studies [50, 51], verified in an experiment very recently [52] that formation of α clusters might hinder a smooth extraction of

*Electronic address: mondal@lpccaen.in2p3.fr

L from Δr_{np} of nuclei with neutron excess. There has also been some debate whether the correlation between L and Δr_{np} should be at saturation or subsaturation densities [15, 53, 54], as the average densities associated to nuclei are lower than the saturation density. A systematic study of the density dependence of this correlation between L and Δr_{np} in models probing different values of Δr_{np} might help to elucidate more information. The present study is intended to do that using relativistic mean field (RMF) models.

The paper is organized as follows. In Sec. II the RMF model used in the present calculation along with the fitting protocol is described. The results obtained in this work are described in Sec. III. Finally, a brief summary is provided in Sec. IV.

II. FORMALISM

The effective RMF Lagrangian used in this work, based on usual Yukawa couplings between the nucleonic field ψ and three mesonic fields, isoscalar-scalar σ , isoscalar-vector ω_μ and isovector-vector ρ_μ and electromagnetic field A_μ along with different couplings among the mesons, is given by [11, 55, 56]

$$\begin{aligned} \mathcal{L}_{int} = & \bar{\psi} \left[g_\sigma \sigma - \gamma^\mu \left(g_\omega \omega_\mu + \frac{1}{2} g_\rho \boldsymbol{\tau} \cdot \boldsymbol{\rho}_\mu + \frac{e}{2} (1 + \tau_3) A_\mu \right) \right] \psi \\ & - \frac{\kappa_3}{6M} g_\sigma m_\sigma^2 \sigma^3 - \frac{\kappa_4}{24M^2} g_\sigma^2 m_\sigma^2 \sigma^4 + \frac{1}{24} \zeta_0 g_\omega^2 (\omega_\mu \omega^\mu)^2 \\ & + \frac{\eta_{2\rho}}{4M^2} g_\omega^2 m_\rho^2 \omega_\mu \omega^\mu \boldsymbol{\rho}_\nu \boldsymbol{\rho}^\nu. \end{aligned}$$

m_σ , m_ω and m_ρ are the masses of the σ , ω and ρ mesons, respectively. The values of $m_\omega = 782.5$ MeV and $m_\rho = 763$ MeV are kept fixed in this calculation. The values of m_σ along with other coupling constants in Eq. (2) *e.g.* $g_\sigma, g_\omega, g_\rho, \kappa_3, \kappa_4, \zeta_0$ and $\eta_{2\rho}$ are fitted to experimental data optimizing an objective function. The cross-coupling between the ω_μ and ρ_μ mesons, with coupling constant $\eta_{2\rho}$, can facilitate one to obtain models with different density dependence of symmetry energy (and eventually different Δr_{np}), but keeping the isoscalar behavior very similar [47, 57].

Four different models were obtained, namely, MOD16, MOD18, MOD19 and MOD23 by fitting binding energies BE and charge radii r_{ch} of 12 closed-shell spherical nuclei across the whole nuclear chart, along with the value of Δr_{np} in ^{208}Pb fixed to four different values *viz.* 0.16, 0.18, 0.19 and 0.23 fm, respectively. The goal of this systematic way of fixing Δr_{np} in ^{208}Pb is to study their effects in different symmetry energy parameters as a function of density, in particular, how it affects the extraction of the L parameter from the correlation between L and Δr_{np} in ^{208}Pb . The objective function minimized to optimize the different coupling constants in Eq. (2) is given by,

$$\chi^2(\mathbf{p}) = \frac{1}{N_d - N_p} \sum_{i=1}^{N_d} \left(\frac{\mathcal{O}_i^{exp} - \mathcal{O}_i^{th}(\mathbf{p})}{\Delta \mathcal{O}_i} \right)^2. \quad (3)$$

The number of experimental data points is N_d and the number of fitted parameters is N_p . The experimental and the corresponding theoretically obtained values of an observable are \mathcal{O}_i^{exp} and $\mathcal{O}_i^{th}(\mathbf{p})$, respectively. $\Delta \mathcal{O}_i$ is the adopted error of an observable. The minimum value of the objective function χ_0^2 corresponds to the χ^2 at \mathbf{p}_0 ; \mathbf{p}_0 being the optimal values of the parameters. Once the objective function is minimized, one can calculate the covariance between two quantities \mathcal{A} and \mathcal{B} (or variance putting $\mathcal{A} = \mathcal{B}$) as [58],

$$\overline{\Delta \mathcal{A} \Delta \mathcal{B}} = \sum_{\alpha\beta} \left(\frac{\partial \mathcal{A}}{\partial p_\alpha} \right)_{\mathbf{p}_0} C_{\alpha\beta}^{-1} \left(\frac{\partial \mathcal{B}}{\partial p_\beta} \right)_{\mathbf{p}_0}. \quad (4)$$

The correlation coefficient between \mathcal{A} and \mathcal{B} is specified by

$$c_{AB} = \frac{\overline{\Delta \mathcal{A} \Delta \mathcal{B}}}{\sqrt{\overline{\Delta \mathcal{A}^2} \overline{\Delta \mathcal{B}^2}}}. \quad (5)$$

One should note that \mathcal{A} and \mathcal{B} can be observables as well as parameters. An inverted element of the curvature matrix $C_{\alpha\beta}^{-1}$ appearing in Eq. (4) is connected to the χ^2 as,

$$C_{\alpha\beta} = \frac{1}{2} \left(\frac{\partial^2 \chi^2(\mathbf{p})}{\partial p_\alpha \partial p_\beta} \right)_{\mathbf{p}_0}. \quad (6)$$

In Table I, different observables \mathcal{O} fitted in the present work, their experimental values [59, 60], adopted errors on them ($\Delta \mathcal{O}$) [61], along with their fitted values are provided. The χ_0^2 values for all the four models obtained here are very similar, lying in between 0.7 and 0.8, which ensures a good quality of the fit for all the four models.

With the optimized set of parameters, symmetry energy as a function of density can be calculated using the Lagrangian described in Eq. (2) as

$$C_{sym}(\rho) = \frac{k_F^2}{6(k_F^2 + M^{*2})^{1/2}} + \frac{g_\rho^2}{12\pi^2} \frac{k_F^3}{m_\rho^{*2}}, \quad (7)$$

$$\text{with, } M^* = M - g_\sigma \sigma, \quad (8)$$

$$\text{and, } m_\rho^{*2} = m_\rho^2 \left(1 + \frac{1}{2M^2} \eta_{2\rho} g_\omega^2 \omega^2 \right). \quad (9)$$

Here, k_F is nucleon Fermi-momentum connected to the density as, $k_F = \left(\frac{3\pi^2 \rho}{2} \right)^{1/3}$; M^* and M are Dirac effective mass and free mass of nucleon, respectively; m_ρ^* is the effective mass of ρ meson. The kinetic part of the symmetry energy C_{sym} in Eq. (7) depends on the Dirac effective mass, which depends on the σ field along with the coupling constant g_σ . The interaction part depends on the isovector coupling constants g_ρ and $\eta_{2\rho}$ through the effective mass of ρ meson in Eq. (9).

III. RESULTS AND DISCUSSIONS

In Fig. 1, symmetry energy C_{sym} (Fig. 1(a)) and density slope parameter L (Fig. 1(b)) as a function of

TABLE I: Observables \mathcal{O} , adopted errors on them $\Delta\mathcal{O}$, corresponding experimental data (Expt.) [59, 60] and their best-fit values for MOD16, MOD18, MOD19 and MOD23. BE and r_{ch} corresponds to binding energy and charge radius of a nucleus, respectively and Δr_{np} is the neutron-skin thickness of the corresponding nucleus. Values of BE are given in units of MeV and r_{ch} and Δr_{np} in fm.

	\mathcal{O}	$\Delta\mathcal{O}$	Expt.	MOD16	MOD18	MOD19	MOD23
^{16}O	BE	4.0	127.62	128.22	128.12	127.99	127.80
	r_{ch}	0.04	2.699	2.693	2.697	2.700	2.703
^{40}Ca	BE	3.0	342.05	343.41	343.47	343.31	343.27
	r_{ch}	0.02	3.478	3.448	3.452	3.455	3.458
^{48}Ca	BE	1.0	416.00	415.08	415.12	415.09	415.18
	r_{ch}	0.04	3.477	3.437	3.437	3.437	3.437
^{56}Ni	BE	5.0	483.99	484.42	484.13	484.10	483.37
	r_{ch}	0.18	3.750	3.682	3.686	3.688	3.699
^{68}Ni	BE	2.0	590.41	592.42	592.65	592.64	592.81
^{90}Zr	BE	1.0	783.90	783.19	783.16	783.08	783.09
	r_{ch}	0.02	4.269	4.263	4.263	4.264	4.265
^{100}Sn	BE	2.0	825.30	828.00	828.00	828.12	828.06
^{116}Sn	BE	2.0	988.68	986.97	987.13	987.33	987.55
	r_{ch}	0.18	4.625	4.622	4.621	4.621	4.620
^{132}Sn	BE	1.0	1102.84	1102.87	1102.88	1102.95	1103.07
	r_{ch}	0.02	4.709	4.713	4.710	4.709	4.707
^{144}Sm	BE	2.0	1195.73	1195.90	1195.86	1195.81	1196.12
	r_{ch}	0.02	4.952	4.953	4.954	4.954	4.955
^{208}Pb	BE	1.0	1636.43	1636.64	1636.59	1636.55	1636.42
	r_{ch}	0.02	5.501	5.531	5.529	5.529	5.528
	Δr_{np}	0.01	-	0.163	0.182	0.192	0.230

density are plotted for the four models MOD16, MOD18, MOD19 and MOD23 as discussed before. The behavior of C_{sym} varies slightly going from MOD16 to MOD23, becoming slightly stiffer in the latter. All the four models in discussion have a crossover at around $\rho \simeq 0.1 \text{ fm}^{-3}$, with $C_{sym}(\rho = 0.1) \approx 24 \text{ MeV}$. This is not surprising keeping in mind the fact that the finite nuclei constrain the symmetry energy at a subsaturation density $\sim 0.7\rho_0$ with its value $\sim 24 \text{ MeV}$ [62]. In contrast, density slope parameter L varies the most around this subsaturation density for the models considered. For MOD16, L has a decreasing trend till $\rho \sim 0.1 \text{ fm}^{-3}$ after which it keeps increasing. On the other extreme MOD23 shows almost a monotonous increasing trend in L with density.

In Fig. 2, mass-radius relation of a neutron star, calculated by solving the Tolman-Oppenheimer-Volkoff (TOV) equations using the Lagrangian in Eq. (2), is plotted for all the four models obtained in this work (see Table I). The equation of state (EoS) of NS gets stiffer with increasing value of $L(\rho_0)$ [67]. One can observe an overall increase in the radii obtained in the models with bigger Δr_{np} in ^{208}Pb , as Δr_{np} and $L(\rho_0)$ are linearly correlated to each other. For reference, the constraint on the mass of pulsar PSR J0348+0432 ($= 2.01 \pm 0.04 M_\odot$) obtained

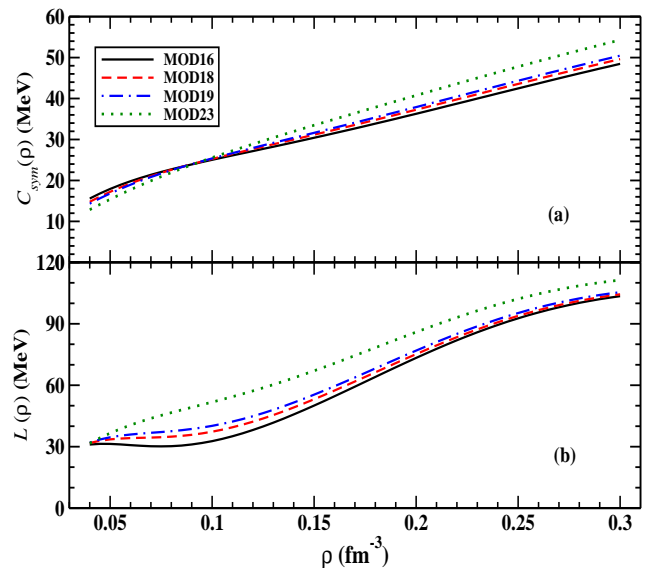


FIG. 1: (Color online) Symmetry energy C_{sym} and density slope parameter L plotted as a function of density ρ obtained with MOD16, MOD18, MOD19 and MOD23.

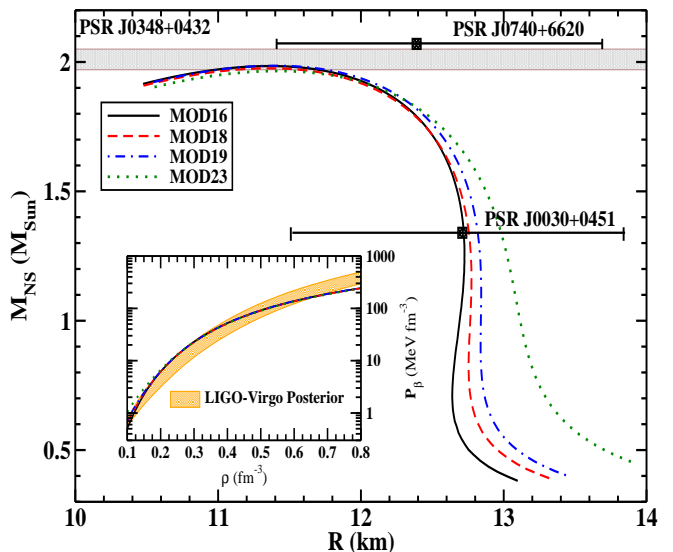


FIG. 2: (Color online) Mass-radius relation for neutron stars obtained with MOD16, MOD18, MOD19 and MOD23. The constraints on the mass for pulsar PSR J0348+0432 ($= 2.01 \pm 0.04 M_\odot$) obtained from radio astronomy observation [63] is given as the grey shaded region. Bounds on the radii from the observations of pulsars PSR J0030+0451 and PSR J0740+6620 by NICER [64, 65] collaboration are also indicated. (Inset): The pressure on the beta-equilibrated matter from the four models along with the posterior band from LIGO-Virgo [66] collaboration.

from radio astronomy using the Shapiro delay technique [63] is provided in Fig. 2. All the models marginally satisfy the constraint provided by this observation. Overall, pretty similar features are observed in M - R plane for all the four models obtained in the present analysis, especially the heavier NSs have almost same radii in each model. Constraints on the radii of pulsars PSR J0030+0451 and PSR J0740+6620 obtained from NICER collaboration [64, 65] are also provided for comparison. The constraint on the heavier star is fairly away from the models considered, however, if the two dimensional joint posterior for the mass-radius is taken into account, there might be a little overlap among them [68]. In the inset of Fig. 2, the pressure of beta equilibrated matter $P_\beta(\rho)$ is plotted as a function of density for the four models obtained in this work, simultaneously with the posterior predicted by the LIGO-Virgo collaboration [66]. All the models overlap quite consistently with the LIGO-Virgo posterior throughout the concerned density range. It is worthwhile to mention here that for all the four models used in this work, the BPS crust EoS [69] is used below the fixed transition density 0.08 fm^{-3} . A more sophisticated way to deal with the crust-core transition would change the radii of small mass NSs at most by 100 - 200 meters, but it would not change the conclusions made above.

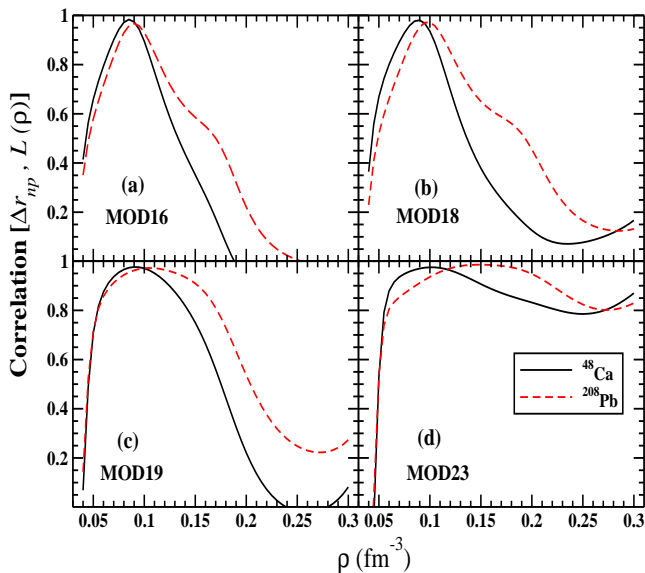


FIG. 3: (Color online) Correlation coefficient between neutron skin Δr_{np} in ^{48}Ca and ^{208}Pb with density slope parameter L is plotted as a function of density ρ for MOD16, MOD18, MOD19 and MOD23.

In Fig. 3, correlation (Eq. (5)) between Δr_{np} of nuclei and density slope parameter L is plotted as a function of density for ^{48}Ca and ^{208}Pb obtained with MOD16, MOD18, MOD19 and MOD23. The results for ^{48}Ca and ^{208}Pb are found to be very similar. This is not surprising keeping in mind the fact that the neutron skins in nu-

clei are quite well correlated among themselves in mean-field models [19]. The correlation coefficient has a very prominent peak, both for ^{48}Ca and ^{208}Pb in the models with lower Δr_{np} (MOD16 or MOD18), which broadens in MOD19 and becomes very wide, appearing almost flat throughout the concerned density range in MOD23. The maximum correlation coefficient between Δr_{np} of ^{208}Pb and L parameter appears at densities 0.09, 0.1, 0.105 and 0.15 fm^{-3} with correlation coefficients 0.967, 0.972, 0.972 and 0.986 for the models MOD16, MOD18, MOD19 and MOD23, respectively. The results for ^{48}Ca and ^{208}Pb are quite similar for all the four models as the correlation coefficient between their corresponding Δr_{np} 's are quite high with the minimum being for MOD19 ~ -0.79 and maximum for MOD18 ~ -0.92 . One can also observe that the peaks for ^{208}Pb are at slightly higher densities for all the cases in comparison to those corresponding to ^{48}Ca . This shows that the average density associated with ^{208}Pb is slightly larger than that in ^{48}Ca . The density dependence of this correlation has some consequences at high densities. It seems that if an RMF model with non-linear couplings among different mesons as in Eq. (2) probes a higher value of Δr_{np} in ^{208}Pb , it probes quite unambiguously the density slope parameter even at suprasaturation densities. Incidentally, the models SINPB and SINPA obtained in a previous work [18] extract very similar Δr_{np} in ^{208}Pb as those obtained from MOD23 and MOD18, respectively. There, the neutron skins were not part of the fit data. However, the density dependence of the correlation between Δr_{np} and L shows almost the same behavior. To understand this in a systematic way, the following analysis is done.

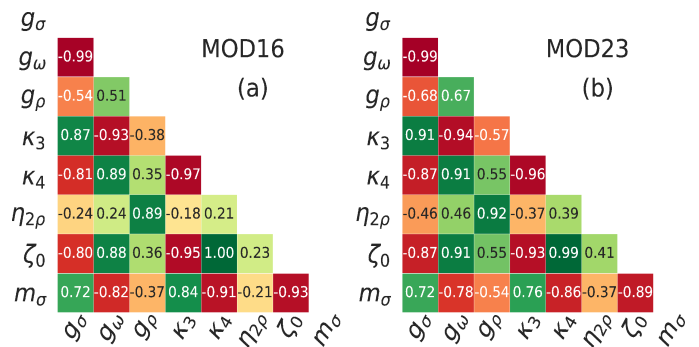


FIG. 4: (Color online) Correlation coefficients obtained with Eq. (5), among different model parameters present in Eq. (2) for MOD16 and MOD23 are displayed in panel (a) and (b), respectively.

Correlation between two observables calculated from a model depends in an involved way on the interdependence of different model parameters among themselves. The correlation coefficients among different parameters in Eq. (2) are plotted in Fig. 4 for MOD16 and MOD23, which represent the two ends of the Δr_{np} probed by the models obtained in the present analysis. There are many strong correlations present among the parameters.

The parameters g_ρ and $\eta_{2\rho}$, which primarily control the isovector part of the interaction, are quite independent from the rest of the parameters (*i.e.* correlation coefficients are small); g_ρ has slightly more dependence on other parameters than $\eta_{2\rho}$. However, they are highly

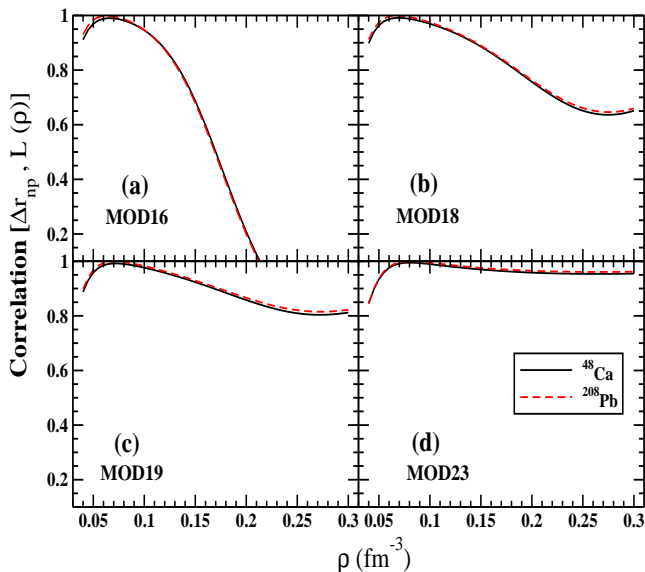


FIG. 5: (Color online) Same as Fig. 3 ignoring the off-diagonal elements present in the correlation matrix for the model parameters which are displayed as in Fig. 4.

correlated to one another. This complex interrelation among the parameters clouds the clear knowledge of the correlation among two observables calculated from these models. This is why understanding the density dependence of the correlation between Δr_{np} and L in Fig. 3 is not very straightforward starting from the correlation among parameters displayed in Fig. 4.

To escape the complex interdependences existing in the multi-dimensional parameter space, as a simplistic assumption, all the inter-correlations existing in Fig. 4 are ignored and the study of Fig. 3 is repeated and presented in Fig. 5. The general behavior of the correlation between Δr_{np} and L as a function of density remains almost unaltered. In models with smaller Δr_{np} for ^{208}Pb , *i.e.* for MOD16 or MOD18, the correlation peaks at a subsaturation density and rapidly decreases at higher densities. The rate of the decrease diminishes when one enters in models with larger Δr_{np} . The correlation coefficients governed by Eqs. (4,5) are now totally dependent on the Jacobians $\left(= \left(\frac{\partial \mathcal{A}}{\partial p_\alpha} \right)_{p_0} \right)$ present in Eq. (4).

In Fig. 6 Jacobians for the density slope parameter L (*i.e.* $\mathcal{A} = L$) is plotted as a function of density for MOD16 and MOD23. As the variation of the Δr_{np} with respect to the parameters does not change with density, the variation in the correlation pattern observed in Fig. 5 (con-

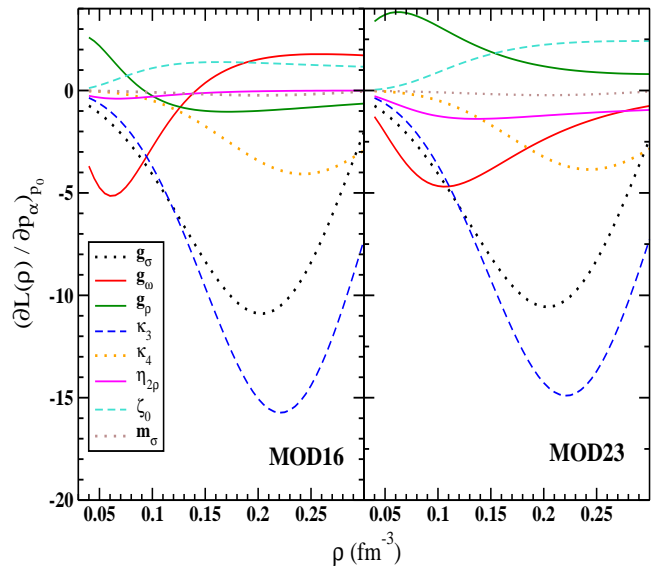


FIG. 6: (Color online) Density dependence of the Jacobians involving density slope parameter L and different model parameters of Eq. (2) are presented for MOD16 and MOD23 in panels (a) and (b), respectively (see text for details).

sequently Fig. 3) is essentially determined by the change in $\left(\frac{\partial L(\rho)}{\partial p_\alpha} \right)_{p_0}$ as a function of density. Also, the Jacobians for Δr_{np} involving all the parameters are found to be very similar for MOD16 and MOD23. It can be seen in Fig. 6 that the primary differences in the density dependences of Jacobians exist corresponding to the parameters g_ω , g_ρ and $\eta_{2\rho}$. The differences in the behavior of Jacobians for density slope parameter L involving g_ρ and $\eta_{2\rho}$ is easy to understand, as they control the isovector part of the interaction (cf. Eqs. (7,9)). The dissimilarity involving g_ω can be realized by looking at the correlation between g_ρ and g_ω in Fig. 4 which transforms from a weak correlation (correlation coefficient 0.51) in MOD16 to a moderate correlation (with coefficient 0.67) in MOD23.

IV. SUMMARY

To summarize, the density dependence of the correlation between neutron skin-thickness and the density slope parameter is systematically studied to shed some light on the nature of the isovector nuclear interaction. Relativistic models of FSU type [11] containing the cross coupling between ω and ρ mesons are used. Models with a wide range of input neutron skin thickness in ^{208}Pb as pseudo-data, along with experimental data on binding energies and charge radii of nuclei across the whole nuclear chart are used. It was observed that the behavior of the symmetry energy and density slope parameter as a function of density or the mass-radius relation in neutron stars is only marginally different for these different models,

so also the relation of pressure in beta-equilibrated matter to density. However, a sharp contrast was found in the density dependence of the correlation between neutron skin in nuclei and the density slope parameter. A model probing a smaller value of neutron skin, shows a peak in the aforementioned correlation at a subsaturation density which progressively flattens and shifts to a high value of density in a model corresponding to a high value of neutron skin. To understand this contrasting behavior, correlation systematics among the model parameters were studied. In a follow up simplistic analysis it was further shown that if the correlation among the model parameters are ignored *a priori*, the overall behavior of the correlation pattern does not change as such. This discloses that the isovector part of the interaction changes its density dependence in models with different values of neutron skin. This might be a specific

feature of the model used in the present analysis (Eq. (2)). Nevertheless, these kind of features should as well be explored in other type of interactions, both relativistic and non-relativistic, as extrapolations of models are often employed to study high density behaviors of nuclear interactions which are primarily obtained by fitting data pertaining to saturation or subsaturation densities.

V. ACKNOWLEDGEMENTS

The author acknowledges Jadunath De and Gagandeep Singh for carefully reading the manuscript and their useful suggestions. This work was partially supported by the IN2P3 Master Project “NewMAC”.

-
- [1] W. D. Myers and W. J. Swiatecki, Nucl. Phys. **A336**, 267 (1980).
- [2] W. D. Myers and W. J. Swiatecki, Ann. Phys. (N. Y.) **55**, 395 (1969).
- [3] P. Möller, W. D. Myers, H. Sagawa, and S. Yoshida, Phys. Rev. Lett **108**, 052501 (2012).
- [4] M. Centelles, X. Roca-Maza, X. Viñas, and M. Warda, Phys. Rev. Lett. **102**, 122502 (2009).
- [5] B. K. Agrawal, J. N. De, and S. K. Samaddar, Phys. Rev. Lett. **109**, 262501 (2012).
- [6] W.-C. Chen and J. Piekarewicz, Phys. Rev. C **90**, 044305 (2014).
- [7] A. W. Steiner, M. Prakash, J. M. Lattimer, and P. Ellis, Phys. Rep. **411**, 325 (2005).
- [8] H.-T. Janka, K. Langanke, A. Marek, G. Martínez-Pinedo, and B. Müller, Phys. Rep. **442**, 38 (2007).
- [9] M. Oertel, M. Hempel, T. Klähn, and S. Typel, Rev. Mod. Phys. **89**, 015007 (2017).
- [10] H. Güven, K. Bozkurt, E. Khan, and J. Margueron, Phys. Rev. C **102**, 015805 (2020).
- [11] B. G. Todd-Rutel and J. Piekarewicz, Phys. Rev. Lett **95**, 122501 (2005).
- [12] J. M. Lattimer, C. J. Pethick, M. Prakash, and P. Haensel, Phys. Rev. Lett. **66**, 2701 (1991).
- [13] X. Roca-Maza, M. Centelles, X. Viñas, and M. Warda, Phys. Rev. Lett. **106**, 252501 (2011).
- [14] H. Jiang, G. J. Fu, Y. M. Zhao, and A. Arima, Phys. Rev. C **85**, 024301 (2012).
- [15] Z. Zhang and L.-W. Chen, Physics Letters B **726**, 234 (2013).
- [16] F. J. Fattoyev, W. G. Newton, and B.-A. Li, Phys. Rev. C **90**, 022801 (2014).
- [17] C. Mondal, B. K. Agrawal, and J. N. De, Phys. Rev. C **92**, 024302 (2015).
- [18] C. Mondal, B. K. Agrawal, J. N. De, and S. K. Samaddar, Phys. Rev. C **93**, 044328 (2016).
- [19] C. Mondal, B. K. Agrawal, M. Centelles, G. Colò, X. Roca-Maza, N. Paar, X. Viñas, S. K. Singh, and S. K. Patra, Phys. Rev. C **93**, 064303 (2016).
- [20] B. A. Brown, Phys. Rev. Lett. **119**, 122502 (2017).
- [21] C. Mondal, B. K. Agrawal, J. N. De, S. K. Samaddar, M. Centelles, and X. Viñas, Phys. Rev. C **96**, 021302(R) (2017).
- [22] J. Margueron, R. Hoffmann Casali, and F. Gulminelli, Phys. Rev. C **97**, 025805 (2018).
- [23] N.-B. Zhang, B.-A. Li, and J. Xu, Astrophys. J. **859**, 90 (2018).
- [24] C. Mondal, B. K. Agrawal, J. N. De, and S. K. Samaddar, International Journal of Modern Physics E **27**, 1850078 (2018).
- [25] W.-J. Xie and B.-A. Li, Astrophys. J. **883**, 174 (2019).
- [26] W.-J. Xie and B.-A. Li, Astrophys. J. **899**, 4 (2020).
- [27] N.-B. Zhang and B.-A. Li, Astrophys. J. **902**, 38 (2020).
- [28] N.-B. Zhang and B.-A. Li, Astrophys. J. **921**, 111 (2021).
- [29] B.-A. Li, B.-J. Cai, W.-J. Xie, and N.-B. Zhang, Universe **7** (2021).
- [30] C. Mondal and F. Gulminelli (2021), arXiv:2111.04520.
- [31] S. M. A. Imam, N. K. Patra, C. Mondal, T. Malik, and B. K. Agrawal (2021), arXiv:2110.15776.
- [32] X. Viñas, M. Centelles, X. Roca-Maza, and M. Warda, The European Physical Journal A **50**, 1 (2014).
- [33] A. Carbone, G. Colò, A. Bracco, L.-G. Cao, P. F. Bortignon, F. Camera, and O. Wieland, Phys. Rev. C **81**, 041301(R) (2010).
- [34] X. Roca-Maza, M. Brenna, B. K. Agrawal, P. F. Bortignon, G. Colò, L.-G. Cao, N. Paar, and D. Vretenar, Phys. Rev. C **87**, 034301 (2013).
- [35] X. Roca-Maza, M. Brenna, G. Colò, M. Centelles, X. Viñas, B. K. Agrawal, N. Paar, D. Vretenar, and J. Piekarewicz, Phys. Rev. C **88**, 024316 (2013).
- [36] T. Malik, B. K. Agrawal, J. N. De, S. K. Samaddar, C. Providência, C. Mondal, and T. K. Jha, Phys. Rev. C **99**, 052801 (2019).
- [37] S. Abrahamyan and et al., Phys. Rev. Lett. **108**, 112502 (2012).
- [38] B. T. Reed, F. J. Fattoyev, C. J. Horowitz, and J. Piekarewicz, Phys. Rev. Lett. **126**, 172503 (2021).
- [39] <https://hallaweb.jlab.org/parity/prex/c-rex2013-v7.pdf> (2014).
- [40] J. Zenihiro and et al., Phys. Rev. C **82**, 044611 (2010).
- [41] A. Krasznahorkay, H. Akimune, A. van den Berg, N. Blasi, S. Brandenburg, M. Csatlós, M. Fujiwara,

- J. Gulyás, M. Harakeh, and M. H. et al., Nucl. Phys. **A731**, 224 (2004).
- [42] B. Klos and *et. al.*, Phys. Rev. C **76**, 014311 (2007).
- [43] E. Friedman and *et. al.*, Hyperfine Interact. **193**, 33 (2009).
- [44] B. A. Brown, Phys. Rev. Lett. **85**, 5296 (2000).
- [45] S. Typel and B. A. Brown, Phys. Rev. C **64**, 027302 (2001).
- [46] C. J. Horowitz and J. Piekarewicz, Phys. Rev. Lett. **86**, 5647 (2001).
- [47] R. Furnstahl, Nucl. Phys. **A706**, 85 (2002).
- [48] S. Yoshida and H. Sagawa, Phys. Rev. C **69**, 024318 (2004).
- [49] L.-W. Chen, C. M. Ko, and B.-A. Li, Phys. Rev. C **72**, 064309 (2005).
- [50] S. Typel, G. Röpke, T. Klähn, D. Blaschke, and H. H. Wolter, Phys. Rev. C **81**, 015803 (2010).
- [51] S. Typel, Phys. Rev. C **89**, 064321 (2014).
- [52] J. T. *et. al.*, Science **371**, 260 (2021).
- [53] Z. Zhang and L.-W. Chen, Phys. Rev. C **90**, 064317 (2014).
- [54] Z. Zhang and L.-W. Chen, Phys. Rev. C **92**, 031301 (2015).
- [55] J. Boguta and A. R. Bodmer, Nucl. Phys. **A292**, 413 (1977).
- [56] J. Boguta and H. Stoecker, Phys.Lett. **B120**, 289 (1983).
- [57] T. Sil, M. Centelles, X. Viñas, and J. Piekarewicz, Phys. Rev. **C71**, 045502 (2005).
- [58] S. Brandt, Statistical and Computational Methods in Data Analysis (Springer, New York, 3rd English edition, 1997).
- [59] M. Wang, G. Audi, A. Wapstra, F. Kondev, M. MacCormick, X. Xu, and B. Pfeiffer, Chinese Physics C **36**, 1603 (2012).
- [60] I. Angeli and K. Marinova, Atomic Data and Nuclear Data Tables **99**, 69 (2013).
- [61] P. Klüpfel, P.-G. Reinhard, T. J. Burvenich, and J. A. Maruhn, Phys. Rev. C **79**, 034310 (2009).
- [62] L. Trippa, G. Colò, and E. Vigezzi, Phys. Rev. C **77**, 061304(R) (2008).
- [63] J. Antoniadis and *et. al.*, Science **340**, 1233232 (2013).
- [64] T. E. Riley, A. L. Watts, P. S. Ray, S. Bogdanov, S. Guillot, S. M. Morsink, A. V. Bilous, Z. Arzoumanian, D. Choudhury, J. S. Deneva, et al., **918**, L27 (2021).
- [65] M. C. Miller, F. K. Lamb, A. J. Dittmann, S. Bogdanov, Z. Arzoumanian, K. C. Gendreau, S. Guillot, W. C. G. Ho, J. M. Lattimer, M. Loewenstein, et al., **918**, L28 (2021).
- [66] B. P. Abbott, R. Abbott, T. D. Abbott, F. Acernese, K. Ackley, C. Adams, T. Adams, P. Addesso, R. X. Adhikari, V. B. Adya, et al. (The LIGO Scientific Collaboration and the Virgo Collaboration), Phys. Rev. Lett. **121**, 161101 (2018).
- [67] R. Cavagnoli, D. P. Menezes, and C. Providência, Phys. Rev. C **84**, 065810 (2011).
- [68] H. Dinh Thi, C. Mondal, and F. Gulminelli, Universe **7**, 373 (2021).
- [69] G. Baym, C. Pethick, and P. Sutherland, Astrophys. J. **170**, 299 (1971).